Constitutive model for soil-rock mixtures in the light of an updated skeleton void ratio concept

Tao Wang, Sihong Liu, Antoine Wautier, François Nicot

Constitutive model for soil-rock mixtures in the light of an updated skeleton void ratio concept

Tao WANG[a], Sihong LIU[a,*], Antoine WAUTIER[b,c], Fran ̧ois NICOT[b,d]

[a]Hohai University, No.1 Xikang Road, Nanjing 210098, China.

[b]Universit é Grenoble Alpes, INRAE, UR ETNA, 2 rue de la Papeterie-BP 76, F-38402 St-Martin-d'Hères, France.

[c]Aix-Marseille University, INRAE, UMR RECOVER, 3275 Rte C ézanne, CS 40061, 13182 Aix-en-Provence, Cedex 5, France.

[d]Universit é Savoie Mont Blanc, EDYTEM (USMB/CNRS), Le Bourget du Lac, France

Email address:

wt@hhu.edu.cn (Tao WANG)

sihongliu@hhu.edu.cn (Sihong LIU, Corresponding author)

antoine.wautier@inrae.fr (Antoine WAUTIER)

francois.nicot@univ-smb.fr (Fran ̧ois NICOT)

Abstract: As a type of special geological body, soil-rock mixtures (SRMs) are widely found in nature and used in civil engineering. Many structures, such as rockfill dams, highways and tunnels have used SRMs as building materials. Proper modelling of SRMs is of great importance to capture the complex behavior of this heterogeneous material. In this manuscript, a simple constitutive model incorporating the skeleton void ratio concept is proposed for SRMs with varying soil contents (*sc*). A prominent feature of the model is a unified description of the behavior of SRMs with varying *sc* such that only model parameters of pure rock and of pure soil are required. After calibration, the model shows a good capacity to predict the stress-strain response of SRMs under a wide range of *sc*, void ratios, and confining pressures. In particular, it captures well the non-associated behavior of rock-dominated SRMs with different *sc*. Furthermore, the *sc*-value is shown to modify the plastic flow direction of the material without influencing its yield surface.

Keywords: Soil-rock mixture; Skeleton void ratio; Soil content; Constitutive modelling; Critical state line; Flow rule direction; Non-associated behavior

1. Introduction

Soil-rock mixtures (SRMs) are heterogeneous materials composed of high-strength rocks, fine-grained soils and pores [37, 38, 42]. SRMs are widely encountered in geotechnical engineering, such as natural slopes [6], waste rocks and tailings from mining [8], clay-aggregate mixtures in rockfill dams [12] and tunnels [14]. The soil content (*sc*) is one of the most important factors governing the mechanical behavior of SRMs [3, 26, 29, 33, 36]. In recent years, many field tests, laboratory tests and numerical simulations have revealed that *sc* greatly affects the shear

strength [4, 16, 23, 37], failure modes [5, 15, 17], stress-dilatancy [4, 33], and critical state parameters of SRMs [25, 33]. Experimental and numerical results both show that at a low *sc*, the mechanical behavior of SRMs is primarily governed by inter-granular friction between rock grains. While at a high *sc* beyond a threshold value $(sc)_{th}$, the mechanical behavior of SRM is primarily governed by friction characteristics of soil grains.

Although some pioneering works has been done on the constitutive modelling of SRMs [7, 17, 26], properly modeling the behavior of this kind of complex heterogeneous materials remains an open challenge [35, 39, 40]. Predicting the mechanical properties SRMs for varying *sc* remains a widely open issue.

1) In most constitutive models, SRMs with different *sc* are indeed treated as different materials with their own *sc*-specific parameters [21, 24, 41]. For example, the shape of the critical state line (CSL) of a SRM and its location depend on *sc*. Therefore, new laboratory tests are required each time *sc* is updated in engineering projects, which results in a waste of time and money.

2) Some models tried to build empirical equations to link model parameters with *sc* [23, 35]. For instance, some empirical equations have been established to fit CSLs of SRMs with *sc* based on experimental data. This method usually introduces new parameters into the constitutive model, i.e., parameters in empirical equations. But, these empirical equations lack of physical meaning and their application to SRMs with different lithology, grain shape and gradation of rock and soils remains questionable.

3) Although many numerical studies have analyzed the microstructure of SRMs, few attempts have been made to incorporate micro- or meso-mechanisms into constitutive models. For

example, Wang et al (2021) [29] found that for rock-dominated SRMs, *sc* does not affect the normal direction of yield surface but it changes the flow rule direction. These findings could be reflected in constitutive models.

In soil constitutive models, the global void ratio *e* has been chosen as one of the main state variable. However, it was found to be an imperfect index to characterize the mechanical behavior of mixed soils like SRMs [29, 33]. This is because such a global index is not able to account for the non-active participation of the soil grains in the force transmission structure within a SRM. Alternatively, skeleton void ratio turns out to be a more appropriate index to reflect the density of SRMs. Skeleton void ratio corresponds to the void ratio of grains constituting the stress-bearing skeleton. In recent studies, this index has shown a strong potential to give unified descriptions of the behavior of SRMs with varying *sc* [29, 35].

The objective of this manuscript is to propose a simple method to predict the stress-strain response of SRMs with varying *sc* incorporating the updated skeleton void ratio concept. It is organized as follows. First, the updated skeleton void ratio for SRMs proposed by Wang et al. (2022) [29] is briefly reviewed. The advantage of using this skeleton void ratio index to characterize critical state lines of SRMs with varying *sc* is then shown. Next, a constitutive model incorporating the skeleton void ratio concept is proposed and the model is validated against experimental results. Eventually, effect of *sc* on the main properties of SRMs is studied and the model capabilities are discussed.

2. Review of an updated skeleton void ratio for SRMs

Wang et al. (2022) [29] proposed an updated skeleton void ratio index for SRMs. The main advantage of this updated skeleton void ratio is that it can consider the effect of gradations of both

soils and rocks. The skeleton void ratio proposed by Thevanayagam (2007) [27] is a special case of the updated skeleton void ratio in which mutual interaction between rock and soil grains during packing is neglected.

According to Wang et al. (2022) [29], the threshold soil content $(sc)_{th}$ that separates the rock-dominated structure and soil-dominated structure is:

$$(sc)_{th} = \frac{e_r - b}{1 + e_r + e_s - a - b} \tag{1}$$

where e_s and e_r are the minimum void ratios of pure soil grains and pure rock grains, respectively. a and b are gradation-related parameters:

$$a = (1 + e_s)\exp(\frac{-{R_d}^{0.5}}{C_{ur}C_{us}}) \tag{2}$$

$$b = e_r\exp(\frac{-R_d}{C_{ur}C_{us}^{0.5}}) \tag{3}$$

where $C_{ur} = \frac{(D_{60})_{rock}}{(D_{10})_{rock}}$ is the coefficient of non-uniformity for the rock fraction, $C_{us} = \frac{(d_{60})_{soil}}{(d_{10})_{soil}}$ is the coefficient of non-uniformity for the soil fraction and $R_d = \frac{(D_{50})_{rock}}{(d_{50})_{soil}}$ is grain size disparity ratio.

For a rock-dominated structure, i.e., $sc<(sc)_{th}$, its skeleton void ratio e_{sk} is given by:

$$e_{sk} = \frac{e + sc}{1 - sc} - \frac{sc(1 + e_s)}{1 - sc}\exp(\frac{-{R_d}^{0.5}}{C_{ur}C_{us}}) \tag{4}$$

For a soil-dominated structure, i.e., $sc>(sc)_{th}$, its skeleton void ratio e_{sk} expresses as:

$$e_{sk} = \frac{e}{sc} - \frac{e_r(1 - sc)}{sc}\exp(\frac{-R_d}{C_{ur}C_{us}^{0.5}}) \tag{5}$$

All the parameters introduced in Equations (1)-(5) can be obtained from simple laboratory sieving and compaction tests.

Wang et al. (2022) [29] found that a rock-dominated (or soil-dominated) SRM has similar stress-strain responses with a pure rock specimen (or a pure soil specimen) if global void ratio of

the pure rock specimen (or pure soil specimen) equals to the skeleton void ratio of the SRM. This important finding is essential to unify descriptions of SRMs with varying soil contents.

3. Characterization of critical state lines of SRMs with updated skeleton void ratio index

The critical state is defined as the state at which the soil continues to deform at constant shear stress and constant volume. It has increasingly been used as a fundamental concept to characterize the strength and deformation properties of soils [2, 20, 22]. Li et al. (1998) [10] found that the critical state lines (CSLs) for cohesionless soils are straight lines in the e–$(p/p_a)^{\xi}$ plane:

$$e_{cr} = e_{\Gamma} - \lambda(p/p_a)^{\xi} \tag{6}$$

Where e_{cr} is critical state void ratio, e_{Γ} is the theoretical critical void ratio at the atmospheric pressure, p_a is the atmospheric pressure, λ is the magnitude of the slope, and ξ is the pressure exponent (with a typical value around 0.7).

Experimental data obtained from conventional drained triaxial tests on SRMs with different soil contents (*sc*=0, 0.1, 0.3, 0.5, 0.7 and 1) under different confining pressures (σ_3=150 kPa, 300 kPa and 600 kPa) conducted by Wang et al. (2022) [29] are adopted here to characterize the CSLs of SRMs with varying *sc* ($C_{ur} = 2.36$, $C_{us} = 7.01$ and R_d=5.46). Detailed test procedures can be found in the quoted reference [29].

Figure 1 gives the CSLs of SRMs with *sc* ranging from 0 to 1 in *e-p* plane. It can be found that SRMs with different *sc* have different CSLs. The CSL move downward from the pure rock specimen until the soil content reaches $(sc)_{th}$ (around 0.54), and then the CSL would move upward to the position of pure soil specimen. According to Wang et al. (2022), all the SRMs were prepared with the same global void ratio. For a rock-dominated specimen, the skeleton void ratio

increases with *sc* and a more contractant behavior is observed. Therefore, the increase in *sc* widens the gap between current void ratio and critical void ratio and leads to the downward shift of the CSL. On the other hand, for a soil-dominated specimen, the increase in *sc* results in a larger skeleton void ratio and a more dilatant behavior, which consequently narrows the gap. Therefore, CSL will move upwards. Critical state line parameters e_Γ and λ are shown in Figure 2. e_Γ and λ are found to be functions of *sc*, which indicates that SRMs with different *sc* should be treated as different materials. Consequently, each SRM has its own CSL in *e*-*p* plane.

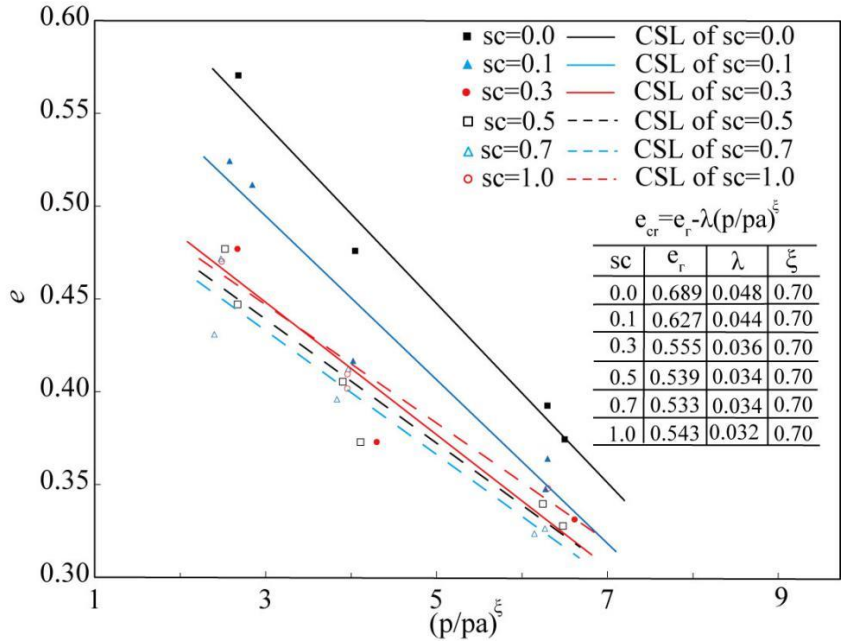

sc	e_r	λ	ξ
0.0	0.689	0.048	0.70
0.1	0.627	0.044	0.70
0.3	0.555	0.036	0.70
0.5	0.539	0.034	0.70
0.7	0.533	0.034	0.70
1.0	0.543	0.032	0.70

Fig. 1 Critical state lines of SRMs with different *sc* drawn in *e*-$(p/p_a)^\xi$ plane

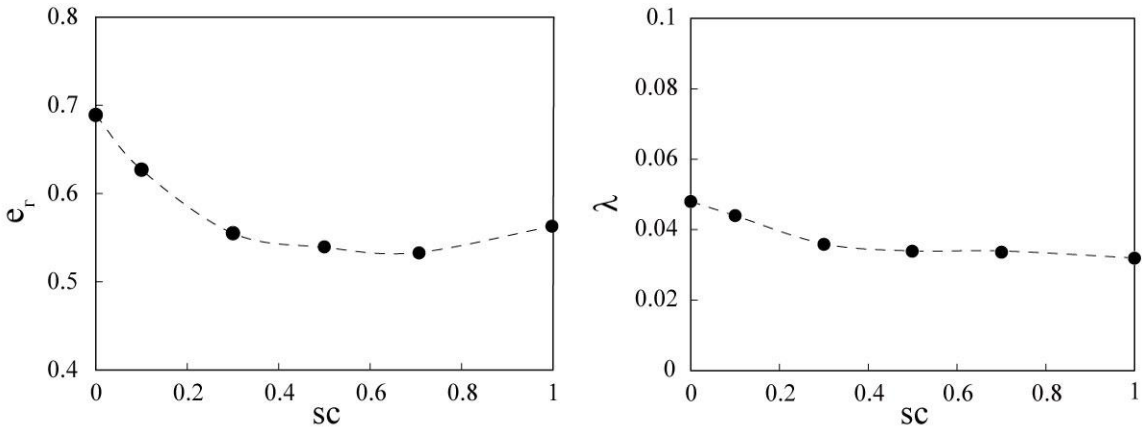

(a) e_Γ **(b)** λ

Fig. 2 Evolution of critical state parameters with *sc*: (a) e_Γ; (b) λ

Critical state data of SRMs with different *sc* are plotted in e_{sk}-p plane in Figure 3. Pure rock and pure soil materials have different CSLs because they have different grain shapes and gradations. Therefore, for a clearer view, we plot separately the critical state data of rock-dominated structure (Figure 3a) and soil-dominated structure (Figure 3b). It can be seen in Figure 3a, that the CSL of pure rock grains (*sc*=0) is shared with SRMs of different *sc* (*sc*=0, 0.1, 0.3 and 0.5<$(sc)_{th}$ = 0.54) for rock-dominated SRMs. Similarly, as shown in Figure 3b, for the soil-dominated specimens (*sc*=0.7, 1>$(sc)_{th}$ = 0.54), the CSL of the pure soil (*sc*=1) is shared with SRM with *sc*=0.7. Consequently, in the e_{sk}-p plane, the critical state of all RSM materials is described either by the CSL of the rock or the SCL of the soil depending whether *sc* is below or above $(sc)_{th}$. This important finding is essential for establishing the constitutive model, as developed in the next section.

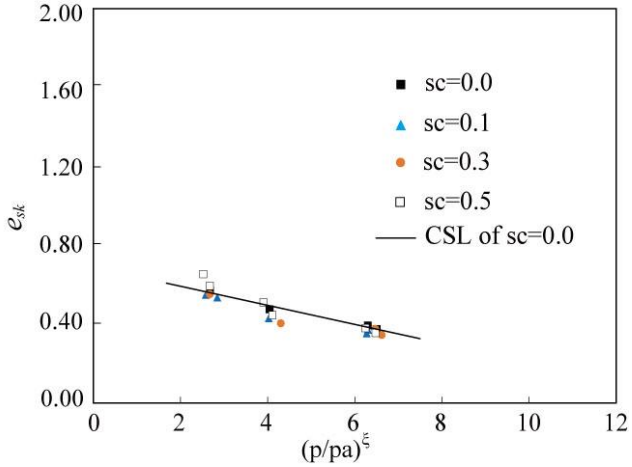

(a) Rock-dominated SRMs

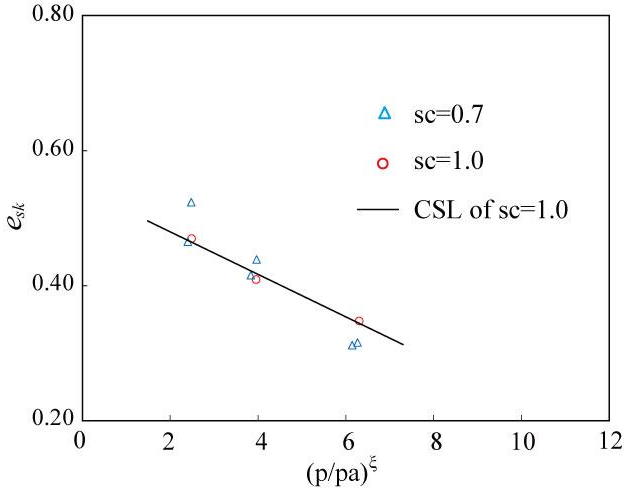

(b) Soil-dominated SRMs

Fig. 1 Critical state lines of SRMs with different *sc* drawn in e_{sk} -$(p/p_a)^{\xi}$ plane

4. A simple constitutive model for SRM using the skeleton void ratio index

The updated skeleton void ratio concept is incorporated into the state-dependent bounding surface model proposed by Li and Dafalias (2000) [9] to capture the stress-strain behaviors of SRMs with different *sc*. The fundamental of this model is that the SRMs and its host rock (or soil) with the same skeleton void ratio should exhibit the same stress-strain behavior, which has been reported by many researchers [28, 29, 35]. The fact that rock-dominated (or soil-dominated) SRMs share the same CSL with pure rock (or pure soil) also suggests to build a unified model for SRMs with varying *sc* from only model parameters of pure rock and pure soil. The constitutive framework is detailed in the following sections.

4.1 Elastic behavior

According to standard elasto-plasticity, a total strain increment $\mathbf{d}\boldsymbol{\varepsilon}$ is additively split into an elastic strain increment $\mathbf{d}\boldsymbol{\varepsilon}^{\boldsymbol{e}}$ and a plastic strain increment $\mathbf{d}\boldsymbol{\varepsilon}^{\boldsymbol{p}}$:

$$\mathbf{d}\boldsymbol{\varepsilon} = \mathbf{d}\boldsymbol{\varepsilon}^{\boldsymbol{e}} + \mathbf{d}\boldsymbol{\varepsilon}^{\boldsymbol{p}} \tag{7}$$

158 The volumetric and deviatoric elastic strain increments are given respectively by:

$$\mathrm{d}\varepsilon_v^e = \frac{\mathrm{d}p'}{K} \tag{8}$$

$$\mathrm{d}\varepsilon_d^e = \frac{\mathrm{d}q}{3G} \tag{9}$$

159 where K is the elastic bulk modulus, G is the elastic shear modulus, $\mathrm{p}' = \frac{\sigma_1 + 2\sigma_3}{3}$ is the mean
160 effective stress and $\mathrm{q} = \sigma_1 - \sigma_3$ is the deviatoric stress (σ_1, σ_2, and σ_3 are the principal stress
161 values).

162 G can be estimated following [19]:

$$G = G_0 \frac{(2.97 - e)^2}{(1 + e)} \sqrt{p' p_a} \tag{10}$$

163 where G_0 is an elastic material constant, p_a is the atmospheric pressure, e is the void of the
164 considered material (soil or rock).

165 The elastic bulk moduli K is given by the following relation:

$$K = G \frac{2(1+\nu)}{3(1-2\nu)} \tag{11}$$

166 where ν is the Poison's ratio.

167 The estimation of G_0 and ν can be found in Appendix.

168 4.2 Plastic behavior

169 For the sake of simplicity, the elasto-plastic model proposed by Li and Dafalias (2000) [9] in
170 the triaxial compression stress space is adopted. In this model, the yield surface is given by:

$$f(p', q, \eta) = q - p'\eta_c = 0 \tag{12}$$

171 where η_c is the stress ratio when plasticity activates. In the model of Li and Dafalias (2000) [9]
172 the yield surface is assumed to follow the stress state so that $\eta_c = \eta$. Note that this hypothesis
173 holds as long as plasticity is activated. In case elastic unloading is considered, the model requires
174 some additional mechanism such as a back-stress [13], or a memory of the reversal stress ratio

point [31] which are not considered in the present study.

According to the theory of plasticity, a loading index dL can be defined as:

$$dL = \frac{1}{K_p}\left(\frac{\partial f}{\partial p'}\mathrm{d}p' + \frac{\partial f}{\partial q}\mathrm{d}q\right) = \frac{\mathrm{d}q - \eta_c \mathrm{d}p'}{K_p} = \frac{p'\mathrm{d}\eta}{K_p} \quad \text{since } \eta_c = \eta \tag{13}$$

where K_p is the plastic hardening modulus and is expressed by Li and Dafalias (2000) [9] as:

$$K_p = hG\left(\frac{M}{\eta} - \exp(n\psi)\right) = \frac{hG\exp(n\psi)}{\eta}(M\exp(-n\psi) - \eta) \tag{14}$$

In the above equation, n is a positive model parameter, $h = h_1 - h_2 e_0$ with h_1 and h_2 are model parameters and e_0 the initial void ratio, M is the stress ratio at a critical state and $\psi = e - e_{cr}$ is the state parameter defined by Been and Jefferies (1985) [1] with e the current void ratio and e_{cr} the critical state void ratio for the current p'. When using skeleton void ratio instead of the void ratio, a skeleton state parameter ψ_{sk} is introduced as $\psi_{sk} = e_{sk} - (e_{cr})_{sk}$, as seen in Figure 4. Note that when softening occurs ($K_p < 0$) the plastic multiplier dL is positive (i.e. plasticity is active) when the stress ratio decreases.

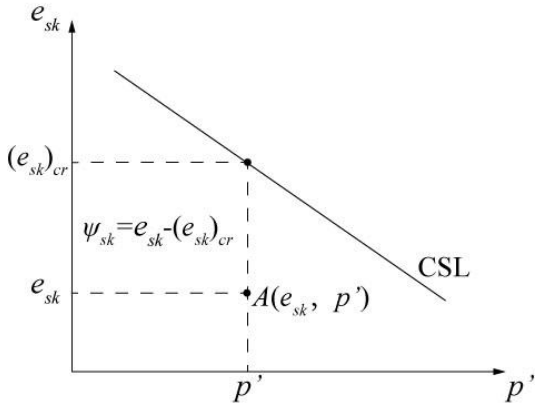

Fig. 4 Definition of skeleton state parameter ψ_{sk}

Since soil-rock mixtures are typical non-associated materials, the non-associated flow rule is adopted to define the plastic strain increments, as follows:

$$\mathrm{d}\varepsilon_d^p = \mathrm{d}L = \frac{p'\mathrm{d}\eta}{K_p} \tag{15}$$

$$\mathrm{d}\varepsilon_v^p = D\mathrm{d}L = \frac{Dp'\mathrm{d}\eta}{K_p} \tag{16}$$

where $d\varepsilon_d^p$ and $d\varepsilon_v^p$ are the plastic deviatoric strain increment and the plastic volumetric strain increment, respectively. The ratio $D = \frac{\mathrm{d}\varepsilon_v^p}{|\mathrm{d}\varepsilon_d^p|}$ evaluates the amplitude of the dilatancy and can be chosen as follows:

$$D = \frac{d_0}{M}[M\exp(m\psi) - \eta] \tag{17}$$

where d_0 and m are model parameters. For associated flow rule, $D = \frac{\mathrm{d}\varepsilon_v^p}{\mathrm{d}\varepsilon_d^p} = \frac{\frac{\partial f}{\partial p}}{\frac{\partial f}{\partial q}} = -\eta_c$.

Therefore, for dL>0, the following expressions can be derived for both incremental deviatoric and volumetric strains:

$$\mathrm{d}\varepsilon_d = \mathrm{d}\varepsilon_d^e + \mathrm{d}\varepsilon_d^p = \frac{\mathrm{d}q}{3G} + \frac{P'\mathrm{d}\eta}{K_p} = \left(\frac{1}{3G} + \frac{1}{K_p}\right)\mathrm{d}q - \frac{\eta}{K_p}\mathrm{d}p' \tag{18}$$

$$\mathrm{d}\varepsilon_v = \mathrm{d}\varepsilon_v^e + \mathrm{d}\varepsilon_v^p = \frac{\mathrm{d}p'}{K} + D\mathrm{d}\varepsilon_q^p = \frac{D}{K_p}\mathrm{d}q + \left(\frac{1}{K} - \frac{D\eta}{K_p}\right)\mathrm{d}p' \tag{19}$$

Equations (18) and (19) set up the relationship between stain and stress increments. Eventually, an elastoplastic constitutive relation is derived in a matrix form:

$$\begin{Bmatrix}\mathrm{d}q\\ \mathrm{d}p'\end{Bmatrix} = \left[\begin{pmatrix}3G & 0\\ 0 & K\end{pmatrix} - \frac{h(dL)}{K_p+3G-K\eta D}\begin{pmatrix}9G^2 & -3KG\eta\\ 3KGD & -K^2\eta D\end{pmatrix}\right]\begin{Bmatrix}\mathrm{d}\varepsilon_q\\ \mathrm{d}\varepsilon_v\end{Bmatrix} \tag{20}$$

where h(dL) is a Heaviside function with h(L)=1 for dL>0 and h(dL)=0, otherwise (plastic stain exists only when dL is positive). Note that equation (20) is given in the plane $(\mathrm{d}p', \mathrm{d}q)$ and the dual plane $(\mathrm{d}\varepsilon_v, \mathrm{d}\varepsilon_q)$. It can be generalized to any kind of incremental stress and strain tensors by assuming coaxiality between incremental stress and strain.

4.3 Model parameters

To summarize, the proposed model includes eleven model parameters, all of them being calibrated from drained triaxial tests under different confining pressures: (1) Two elastic parameters, i.e. G_0 and ν; (2) Four critical state parameters, i.e. M, e_Γ, λ and ξ; (3) Two dilatancy parameters, i.e. d_0, m; (4) Three hardening parameters, i.e. h_1, h_2 and n.

It should be noted that no new parameters have been introduced into this approach. Skeleton

void ratio e_{sk} of SRMs with different *sc* are adopted to replace global void ratio *e* in the above-mentioned equations. Accordingly, skeleton state parameter ψ_{sk} is used in the place of ψ. By doing so, the behavior of SRMs with varying *sc* can be predicted from only the model parameters of pure rock and pure soil. Thus, SRMs with different *sc* should no longer be treated as different materials and only require own *sc*-specific model parameters.

5. Model performance

In this section, the experimental data obtained by Wang et al. (2022) [29] are adopted to test the performance of the constitutive model introduced above. In reference [29], conventional drained triaxial tests on soil-rock mixtures with *sc*=0, 0.1, 0.3, 0.5, 0.7 and 1 were conducted under three different confining pressures (σ_3=150 kPa, 300 kPa and 600 kPa).

The threshold soil content $(sc)_{th}$ of the SRM used in [26] is 0.54. The threshold soil content is larger than that reported by other researchers. The reason may be the use of angular gravel in their tests, which cause large voids among rock grains. Therefore, SRMs with *sc*=0.1, 0.3 and 0.5 are rock-dominated SRMs, whose behavior can be predicted from model parameters of pure rock, while stress-strain responses of soil-dominated SRM (i.e., *sc*=0.7) can be predicted from the model parameters of pure soil. The calibrated model parameters of the pure rock and pure soil used in [26] are listed in Table 1. The description of the calibration process of model parameters is reported in Appendix.

Table 1. Model parameters calibrated for pure rock (*sc*=0) and pure soil (*sc*=1).

	Elastic parameters	Critical state parameters	Dilatancy parameters	Hardening parameters

Pure rock (*sc*=0)	$G_0 = 200$ $\nu = 0.32$	$M = 1.79$ $e_\Gamma = 0.689$ $\lambda = 0.048$ $\xi = 0.70$	$d_0 = 1.5$ $m = -1.0$	$h_1 = 0.2$ $h_2 = 0.3$ $n = 3.9$
Pure soil (*sc*=1)	$G_0 = 50$ $\nu = 0.25$	$M = 1.70$ $e_\Gamma = 0.543$ $\lambda = 0.032$ $\xi = 0.70$	$d_0 = 1.8$ $m = 0.2$	$h_1 = 0.6$ $h_2 = 2.0$ $n = 7.0$

5.1 Stress-strain-volume behavior

Figures 5 and 6 display comparisons between predicted results and experimental results in terms of stress ratios, volumetric strains and evolutions of global void ratios for SRMs with varying *sc*. It can be seen that the stress ratio and the volumetric strain can be fairly described by the model for drained shear responses of SRMs under a range of confining stresses and soil contents.

SRMs exhibit post peak strain softening and volumetric expansion at a low confining pressure i.e., σ_3=150 kPa. While at higher confining pressures, i.e., σ_3=300 kPa and 600 kPa, SRMs present strain hardening and the volumetric contraction. As shown in Figure 5, the model can capture both the stress and the volumetric strain behaviors of SRMs with varying *sc*, e.g., the strain hardening, the volumetric contraction, the strain softening, and the volumetric expansion. In addition, the predicted peak stress ratio, critical stress ratio, phase transformation point from contraction to dilatancy, ultimate volumetric strain, and evolution of void ratio agree well with experimental results.

Some discrepancies between simulated and experimental curves may be observed when *sc* is close to $(sc)_{th}$, i.e., when *sc*=0.3 and 0.5. One possible reason for this phenomenon is that when *sc* is close to $(sc)_{th}$ a dual skeleton structure is formed in SRM which is composed of both rock and

soil grains. Therefore, some discrepancies may occur if we still regard the SRMs as pure rock-skeleton structure or soil-skeleton structure.

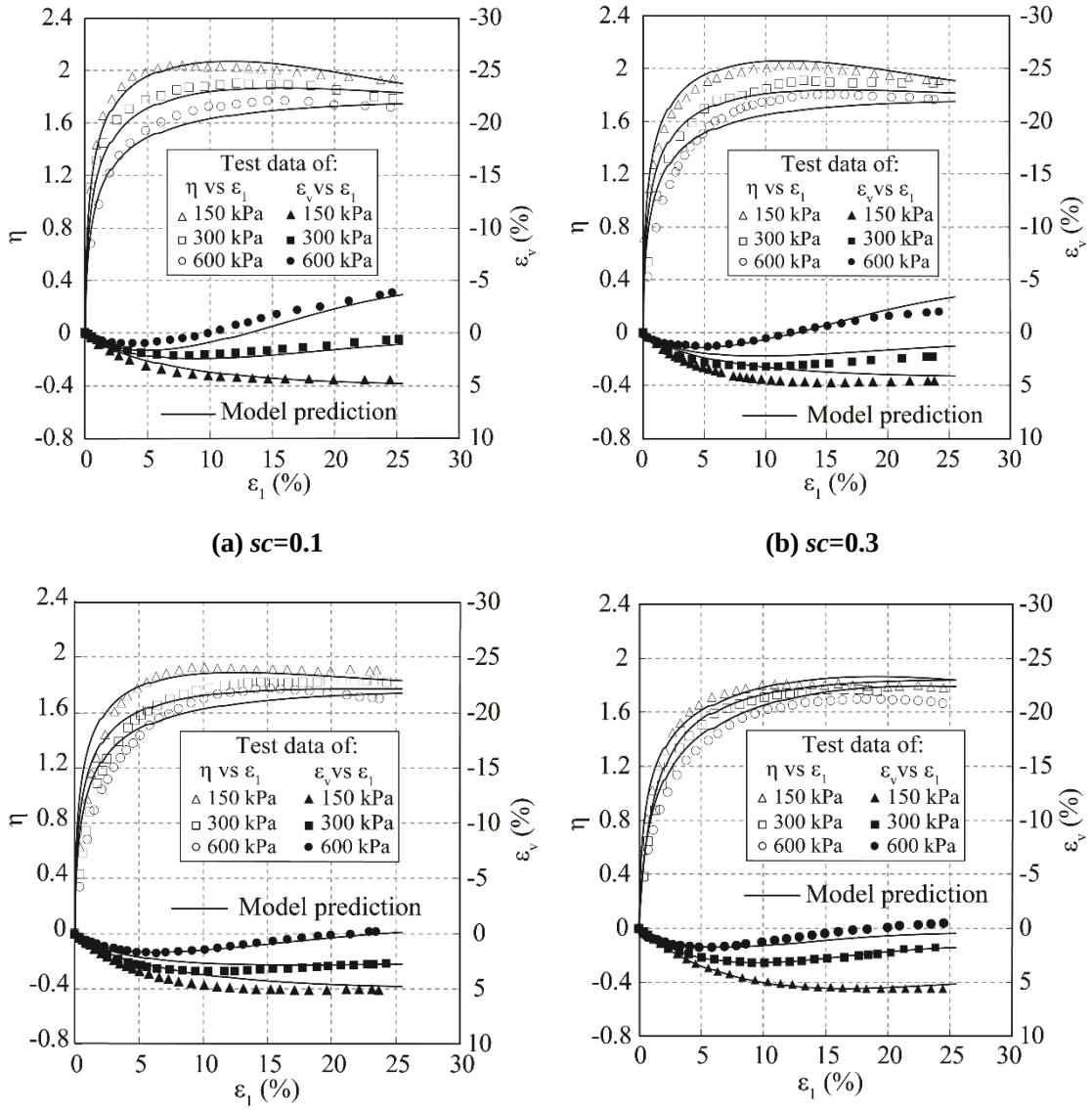

(a) *sc*=0.1 **(b) *sc*=0.3**

(c) *sc*=0.5 **(d) *sc*=0.7**

Fig. 5 Comparison between predicted results and experimental results in terms of stress ratio versus axial strain and volumetric strain versus axial strain.

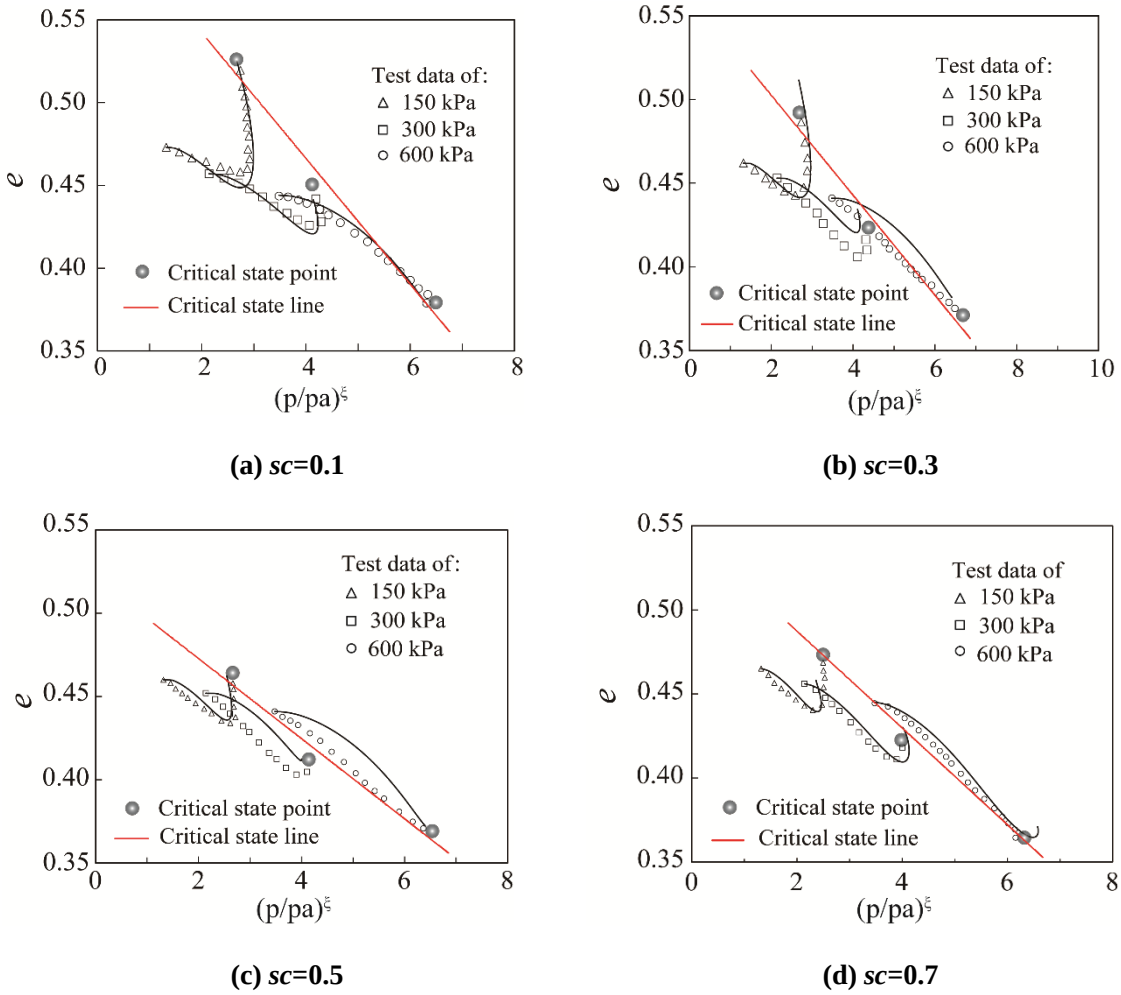

(a) *sc*=0.1 **(b) *sc*=0.3**

(c) *sc*=0.5 **(d) *sc*=0.7**

Fig. 6 Comparison between predicted results and experimental results in terms of void ratio versus mean pressure

5.2 Mobilized friction angle

In this section, we assess whether our model can properly reflect the mobilized friction angle of SRMs with different *sc* and confining pressures. The mobilized friction angle φ_m is defined as:

$$\sin\varphi_m = \frac{\sigma_1 - \sigma_3}{\sigma_1 + \sigma_3} \tag{21}$$

where σ_1 and σ_3 are major and minor principal stresses, respectively. In axisymmetric conditions, $\sin\varphi_m = \frac{3\eta}{6+\eta}$.

Figure 7 shows the comparisons between test results and model predictions in terms of the

252 relationship between mobilized friction angle φ_m and void ratio *e*. It can be seen that the model

253 captures well the variations of φ_m with *e* for SRMs under different confining pressures, although

254 the model slightly overestimates φ_m at high confining pressure of 600 kPa when *sc*=0.3 and 0.5.

255 This might be due to the formation of a dual skeleton structure in the specimen with both rock and

256 soil grains when *sc*=0.3 and 0.5 (close $(sc)_{th}$ = 0.54).

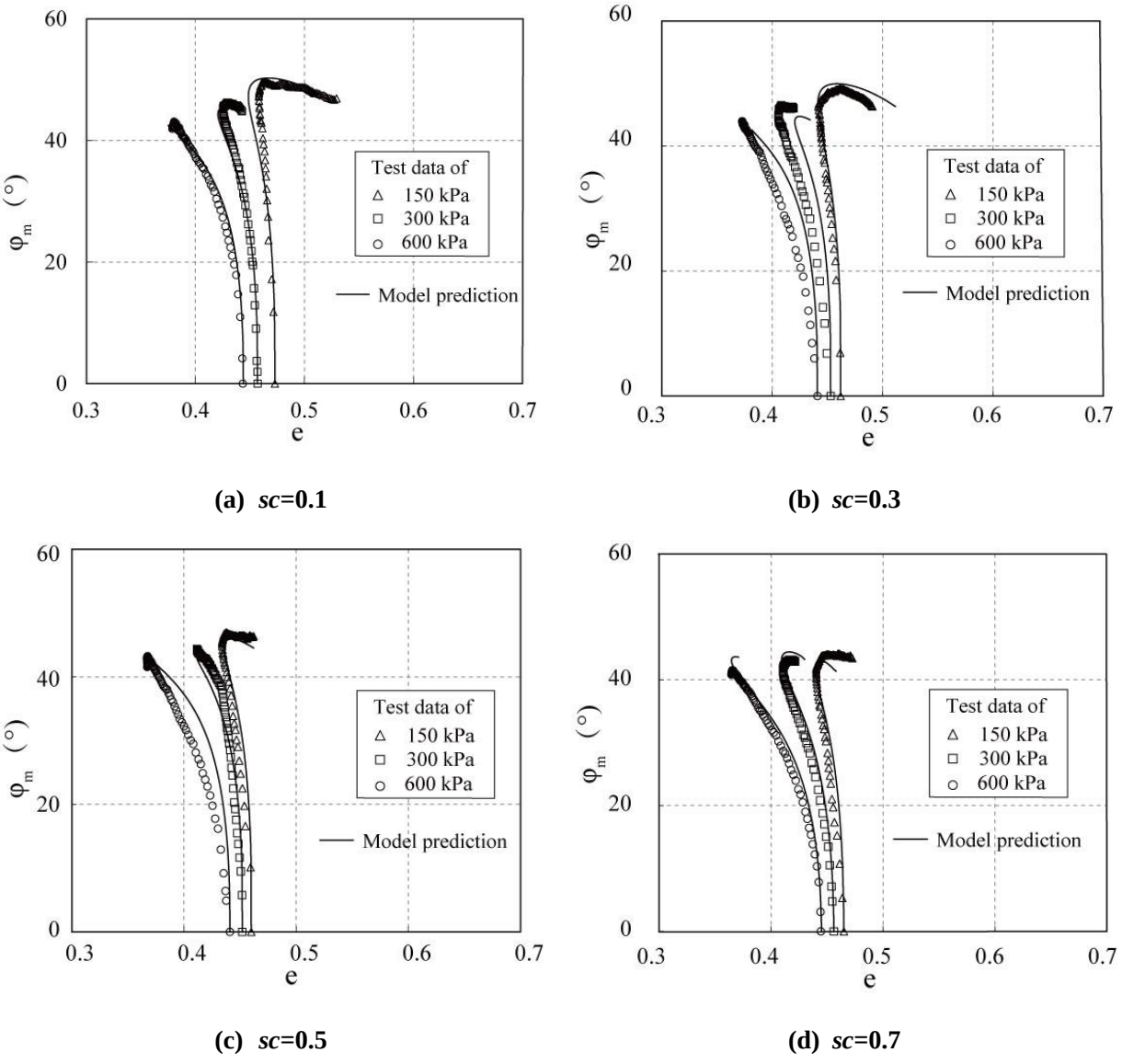

(a) *sc*=0.1 **(b) *sc*=0.3**

(c) *sc*=0.5 **(d) *sc*=0.7**

Fig. 7 Comparison between predicted results and experimental results in terms of void ratio versus mobilized friction angle φ_m.

6. Effect of soil content on essential behavior of SRMs

6.1 Effect of *sc* on the non-associate behavior

In order to investigate the effect of *sc* on the non-associated behavior of rock-dominated SRMs, the yield surface normal direction α and flow rule direction β can be introduced as illustrated in Figure 8 in the p-q plane and dual $d\varepsilon_v$-$d\varepsilon_d$ plane for a non-associated flow rule with on a yield surface corresponding to Mohr-Coulomb criterion.

$$\tan\alpha = \frac{q}{p} \tag{22}$$

$$\tan\beta = -\frac{d\varepsilon_v}{d\varepsilon_d} \tag{23}$$

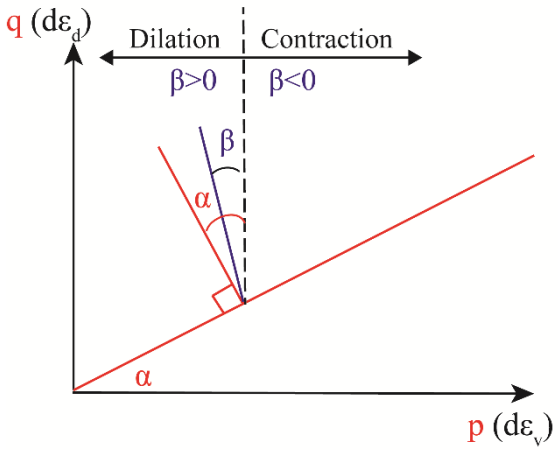

Fig. 8 Schematic diagram of normal to yield surface and flow rule direction. Both directions can be formulated with respect to angles α and β. The sign convention of soil mechanics is applied (positive stress in compression and positive strain in contraction).

Knowing the model yield function from equation (12), the normal direction to the yield surface α and flow rule direction β are shown in Figure 9 for rock-dominated SRMs (*sc*=0, 0.1

and 0.3) under confining pressures of 150 kPa, 300 kPa and 600 kPa. It can be seen that for each confining pressure, when compared at the same stress ratio η, α of SRMs with different *sc* are the same, indicating a non-dependence of the normal yield surface direction upon *sc*. On the other hand, β increases with *sc* (positive for dilation and negative for contraction), indicating that SRMs exhibit more dilantancy with the increase of *sc*. Therefore, the angle between normal direction of yield and flow rule direction decreases with *sc*, meaning the non-associate character is less pronounced with *sc*.

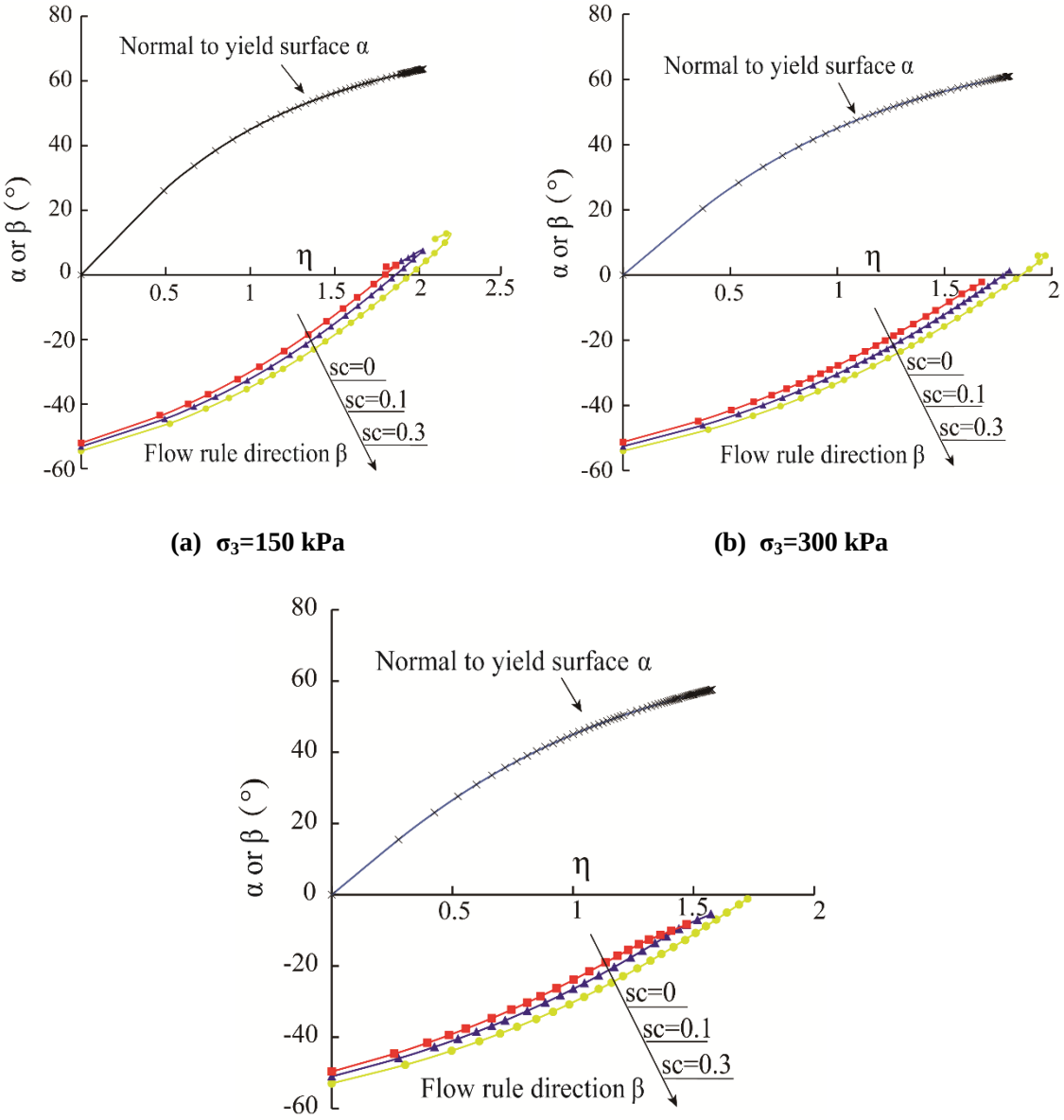

(a) σ_3=150 kPa **(b) σ_3=300 kPa**

(c) σ_3=600 kPa

Fig. 9 Normal to yield surface and flow rule direction of rock-dominated SRMs with *sc*=0, 0.1 and 0.3 under confining pressure of 150 kPa, 300 kPa and 600 kPa.

277 The mesoscale origin of plastic deformation in SRMs is illustrated in Figure 10. The
278 macroscopic activation of the plastic behavior corresponds to substantial grain rearrangements
279 resulting from the collapse of preexisting force chains oriented in the principal stress direction (the
280 vertical direction in Figure 10). Once they collapse, the specimen shrinks in this direction together
281 with smaller expansion in the lateral direction. When small grains fill the pore space, the vertical
282 contraction decreases, whereas the lateral expansion is mostly unaffected. Therefore, the increase
283 in soil content is expected to enhance dilatancy in SRMs specimens.

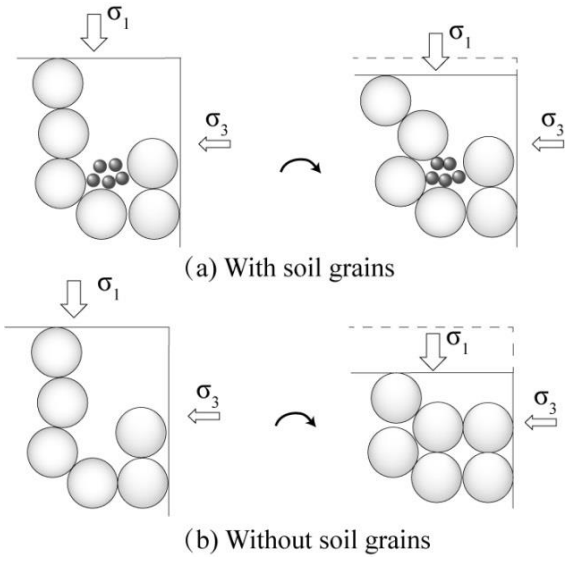

284

285 **Fig. 10** Illustration of the plastic deformation with and without soil grains [29]

286 The conceptual model of Figure 10 was proved with DEM results by Wang et al. (2021) [29]
287 and Wautier et al. (2019) [32]. Wang et al. (2021) [29] found that for rock-dominated SRMs, *sc*
288 does not affect the normal direction of yield surface but it changes the flow rule direction. For
289 rock-dominated SRMs, the non-associated character is less pronounced with the increase of *sc*, as

shown in Figure 11. It should be noted that the normal directions of yield and plastic potential surfaces shown in Fig. 11 are computed directly from DEM results, while the normal to yield surface in Figure 9 depends on the expression of yield surface selected (e.g., Equation (12)).

Similarly, in the proposed model, soil content is found to affect the flow rule direction but the mechanical state and the yield surface of rock-dominated SRMs are not affected. Indeed, this is an intrinsic property of the elasto-plastic model of Li and Dafalias (2000) [9] used in this study. The model assumes that the yield surface follows the stress state at any time (see Equation 12 where the current stress ratio is used). Consequently, the yield surface is independent of the soil content. The consistency between model predictions and DEM simulations proves the ability of this constitutive model to properly reflect the non-associated properties of SRMs with *sc*.

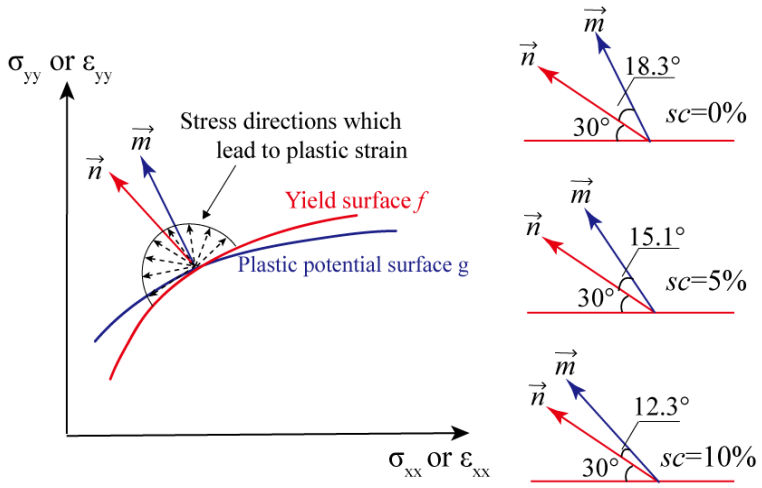

Fig. 11 Schematic diagram of yield surface *f* and plastic potential surface *g* (on the left) and their normal directions $\vec{m}$ and $\vec{n}$ (on the right) for DEM specimens with different *sc* at the same stress ratio η=0.43 (Wang et al., 2021 [29]).

6.2 Effect of *sc* on peak and critical state friction angle

As can be seen in Figure 7, φ_m increases to a peak value φ_p, i.e., peak friction angle, and

306 then decreases to the critical state friction angle φ_{cr} at relatively low confining pressures. Values
307 of φ_p and φ_{cr} of SRMs with varying *sc* are displayed in Figure 12. It can be seen that φ_{cr}
308 almost keeps constant for both rock-dominated structure (at low *sc*) and soil-dominated structure
309 (at high *sc*), while φ_p decreases with *sc* for rock-dominated structure and increases with *sc* for
310 soil-dominated structure. For rock-dominated structures, as a rock skeleton exists, φ_{cr} is
311 primarily governed by intergranular friction between rock grains. Therefore, φ_{cr} is constant for
312 all rock-dominated SRMs. Likewise, for soil-dominated structures, a soil skeleton exists, and
313 φ_{cr} is primarily governed by friction characteristics of soil grains. Therefore, φ_{cr} is also constant
314 for all soil-dominated SRMs. The reason why φ_{cr} in rock-dominated structures is higher than
315 that in soil-dominated structures is that the rock grains used in triaxial tests are more angular than
316 soil grains. However, φ_p is related to the density (in particular e_{sk}) of the initial SRM samples. It
317 is reported in [29] that e_{sk} decreases with *sc* for rock-dominated SRMs and increases with *sc* for
318 soil-dominated SRMs. This explains why φ_p decreases with *sc* for rock-dominated SRMs and
319 increases with *sc* for soil-dominated SRMs.

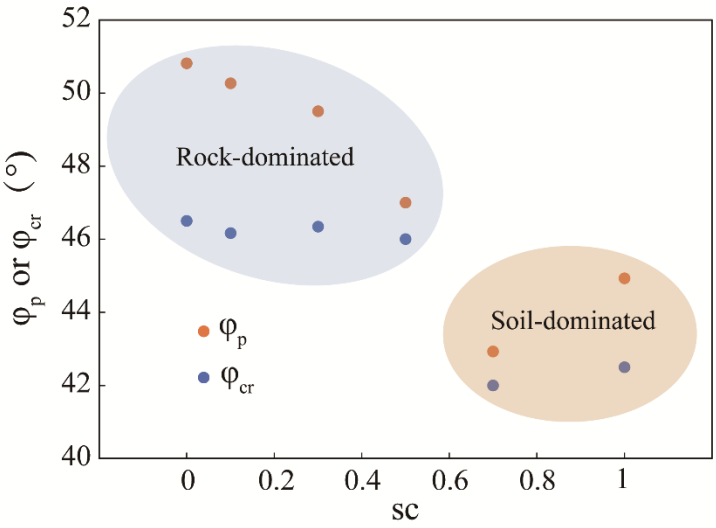

320

321 **Fig. 12 Changes in peak friction angle φ_p and critical friction angle φ_{cr} with *sc***
322 **(σ_3=150kPa)**

7. Closure remarks

The main contribution of this work is the proposal of a simple method to predict the stress-strain responses of SRMs with varying soil contents. This method incorporates the concept of an updated skeleton void ratio. Using this concept, SRMs with different *sc* should no longer be regarded as different materials with their own *sc*-dependent model parameters. Only model parameters of pure rock and of pure soil are required to describe the stress-strain response SRMs with varying *sc*. Our proposal to adopt the skeleton void ratio is generic and can be applied to other constitutive frameworks, ranging from phenomenological models to micro-mechanically based models provided that skeleton parameters (for instance, e_{sk} and ψ_{sk}) are adopted. In this manuscript, the constitutive framework proposed by Li and Dafalias (2000) [9] is adopted as an example to demonstrate the effectiveness of this method. Extending this investigation toward other constitutive frameworks will be considered in future work.

The proposed method demonstrates a satisfying ability for predicting stress-strain responses of SRMs with different soil contents and confining pressures. In addition, it successfully reflects the non-associativity behavior of rock-dominated SRMs. Some discrepancies between simulated and experimental curves are observed when *sc* is close to $(sc)_{th}$. One possible reason for this phenomenon is that a dual skeleton structure composed of both rock and soil grains is formed in SRM when *sc* is close to $(sc)_{th}$. This could be improved in future work by characterizing the complex dual skeleton structure in DEM simulations or X-ray tomography images for instance.

Acknowledgements

This work was supported by National Natural Science Foundation of China (Grant No. U1765205 and No. 51979091). The authors also express their sincere thanks to the International

Research Network GeoMech (IRN GeoMech, CNRS) for promoting stimulating and convivial interactions among researchers.

References

1 Been K, Jefferies MG (1985) A state parameter for soils. *Geotechnique* 35: 99-112

2 Casagrande A (1936) Characteristics of cohesionless soils affecting the stability of slopes and earth fills. J. Boston Society of Civil Engineers 23:13-32

3 Cen D, Huang D, Ren F (2017) Shear deformation and strength of the interphase between the soil–rock mixture and the benched bedrock slope surface. Acta Geotechnica 12: 391-413

4 Chen GX, Wu Q, Sun T, et al (2021) Cyclic behaviors of saturated sand-gravel mixtures under undrained cyclic triaxial loading. *Journal of Earthquake Engineering* 25:756-789

5 Dong H, Peng BC, Gao QF, et al (2021) Study of hidden factors affecting the mechanical behavior of soil–rock mixtures based on abstraction idea. *Acta Geotechnica* 16:595-611

6 Gao WW, Gao W, Hu RL, et al (2018) Microtremor survey and stability analysis of a soil-rock mixture landslide: a case study in Baidian town, China. *Landslides* 15:1951-1961

7 Gobbi, S., Santisi d'Avila, M. P., Lenti, L., Semblat, J. F., & Reiffsteck, P. (2022). Effect of active plastic fine fraction on undrained behavior of binary granular mixtures. International Journal of Geomechanics, 22(1), 06021035.

8 Khalili A, Wijewickreme D, Wilson GW (2010) Mechanical response of highly gap-graded mixtures of waste rock and tailings. Part I: Monotonic shear response. *Canadian Geotechnical Journal* 47:52-565

9 Li XS, Dafalias YF (2000) Dilatancy for cohesionless soils. *Geotechnique* 50: 449-460

10 Li XS, Wang Y (1998) Linear representation of steady-state line for soil. *Journal of geotechnical and geoenvironmental engineering* 124:1215–121

11 Liu HB, Zou DG (2013) Associated generalized plasticity framework for modeling gravelly soils considering particle breakage. *Journal of Engineering Mechanics* 139:606-615

12 Lu Y, Liu SH, Zhang YG, et al (2021) Hydraulic conductivity of gravelly soils with various coarse particle contents subjected to freeze–thaw cycles. *Journal of Hydrology* 598:126302

13 Manzari MT, Dafalias YF (1997) A critical state two-surface plasticity model for sands. Géotechnique 47:255-272

14 Napoli ML, Barbero M, Scavia C (2021) Tunneling in heterogeneous rock masses with a block-in-matrix fabric. *International Journal of Rock Mechanics and Mining Sciences* 138:104655.

15 Ng TT, Zhou W, Chang XL (2017) Effect of particle shape and fine content on the behavior of

binary mixture. *Journal of Engineering Mechanics* 143:C4016008

16 Phan QT, Bui HH, Nguyen GD, & Bouazza A (2021) Effect of particle rolling resistance on drained and undrained behaviour of silty sand. Acta Geotechnica 1-26

17 Porcino DD, Diano V, Triantafyllidis T, & Wichtmann T (2020) Predicting undrained static response of sand with non-plastic fines in terms of equivalent granular state parameter. Acta Geotechnica 15:867-882

18 Rahman, M. M., & Dafalias, Y. F. (2022). Modelling undrained behaviour of sand with fines and fabric anisotropy. Acta Geotechnica, 17(6), 2305-2324.

19 Richart FE (1970) Vibrations of soils and foundations. Prentice Hall. Inc., Englewood Cliffs, New Jersey

20 Roscoe KH, Schofield A, Wroth AP (1958) On the yielding of soils. *Geotechnique* 8:22-53

21 Saberi M, Annan CD, Konrad JM (2017) Constitutive modeling of gravelly soil–structure interface considering particle breakage. *Journal of Engineering Mechanics* 143:04017044

22 Schofield AN, Wroth P (1968) Critical state soil mechanics. London: McGraw-hill Vol. 310

23 Shi XS, Liu K, Yin J (2021) Analysis of mobilized stress ratio of gap-graded granular materials in direct shear state considering coarse fraction effect. *Acta Geotechnica* 6:1801-1814

24 Shi XS, Zhao JD, Gao YF (2021) A homogenization-based state-dependent model for gap-graded granular materials with fine-dominated structure. *International Journal for Numerical and Analytical Methods in Geomechanics* 45:1007-1028

25 Shi XS, Zhao JD, Yin JH, et al (2019) An elastoplastic model for gap-graded soils based on homogenization theory. *International Journal of Solids and Structures* 163:1-14

26 Sun, Z., Chu, J., & Xiao, Y. (2021). Formulation and implementation of an elastoplastic constitutive model for sand - fines mixtures. International Journal for Numerical and Analytical Methods in Geomechanics, 45(18), 2682-2708.

27 Thevanayagam S (2007) Intergrain contact density indices for granular mixes—I: Framework. *Earthquake engineering and engineering vibration* 6:123

28 Thevanayagam S, Mohan S (2000) Intergranular state variables and stress–strain behaviour of silty soils. *Geotechnique* 50:1-23

29 Wang T, Liu SH, Wautier A, Nicot F (2022) An updated skeleton void ratio for gravelly sand mixtures considering the effect of grain size distribution. *Canadian Geotechnical Journal*, 59(1): 12-23.

30 Wang T, Wautier A, Liu SH, Nicot F (2021) How fines content affects granular plasticity of under-filled binary mixtures, Acta Geotechnica, 2021: 1-15.

31 Wang ZL, Dafalias YF, Shen CK (1990) Bounding surface hypoplasticity model for sand. Journal of engineering mechanics 116: 983-1001

32 Wautier A, Bonelli S, Nicot F (2019) Rattlers' contribution to granular plasticity and mechanical stability. *International Journal of Plasticity* 112:172-193

33 Vallejo LE (2021) Interpretation of the limits in shear strength in binary granular mixtures. *Canadian Geotechnical Journal* 38:1097-1104

34 Xiao Y, Sun YF, Hanif KF (2015) A particle-breakage critical state model for rockfill material. *Science China Technological Sciences* 58:1125-1136

35 Xiao Y, Sun YF, Liu HL, et al (2017) Model predictions for behaviors of sand-nonplastic-fines mixtures using equivalent-skeleton void-ratio state index. *Science China Technological Sciences* 60: 878-892

36 Xiong H, Yin Z Y, Zhao J, et al (2021) Investigating the effect of flow direction on suffusion and its impacts on gap-graded granular soils. Acta Geotechnica 16: 399-419

37 Xu WJ, Qiang X, Hu RL (2011) Study on the shear strength of soil–rock mixture by large scale direct shear test. *International Journal of Rock Mechanics and Mining Sciences* 48:1235-1247

38 Yang YT, Sun GH, Zheng H, et al (2019) Investigation of the sequential excavation of a soil-rock-mixture slope using the numerical manifold method[J]. *Engineering Geology* 256: 93-109

39 Yin ZY, Huang HW, Hicher PY (2016) Elastoplastic modeling of sand–silt mixtures. *Soils and Foundations* 56:520-532

40 Yin ZY, Zhao JD, Hicher PY (2014). A micromechanics-based model for sand-silt mixtures. *International journal of solids and structures* 51:1350-1363

41 Zhang G, Zhang JM, Yu Y (2007) Modeling of gravelly soil with multiple lithologic components and its application. *Soils and Foundations* 47:799-810

42 Zhao LH, Huang DL, Zhang SH, et al (2021) A new method for constructing finite difference model of soil-rock mixture slope and its stability analysis. *International Journal of Rock Mechanics and Mining Sciences* 138: 104605

Appendix: Calibration of model parameters

(1) Elastic parameters

The initial elastic shear modulus, G, can be obtained from the experimental data of deviatoric stress, q, versus the deviatoric strain, ε_s when the axial strain is lower than 0.2%. Rearrangement of Equation (10) gives:

$$G_0 = G\frac{(1+e)}{(2.97-e)^2\sqrt{P'P_a}} \tag{A1}$$

The values of the elastic constant, G_0, at various confining pressures, can be determined from Equation (A1). The average value of G_0 under different confining pressures is adopted.

Based on Equations (7)-(11), the Poisson's ratio, ν can be obtained by:

$$\nu = \frac{9\mathrm{d}\varepsilon_s^e - 2\mathrm{d}\varepsilon_v^e}{18\mathrm{d}\varepsilon_s^e + 2d\varepsilon_v^e} \approx \frac{9\varepsilon_s - 2\varepsilon_v}{18\varepsilon_s + 2\varepsilon_s} \tag{A2}$$

(2) Critical state parameters

e_Γ, λ and ξ can be determined by directly fitting the experimental data for the critical state line. The critical state stress ratio M can be obtained by fitting critical state test data in p'-q plane with a function of $q=Mp'$.

(3) Dilatancy parameters

The parameter m is determined from Equation (17) at a phase transformation state, at which D=0, and thus,

$$m = \frac{1}{\psi^d} ln \frac{M^d}{M} \tag{A3}$$

where ψ^d and M^d are the values of ψ and η at the phase transformation state.

Ignoring the small elastic strain, we have:

$$\frac{\mathrm{d}\varepsilon_v}{\mathrm{d}\varepsilon_q} \approx \frac{\mathrm{d}\varepsilon_v^p}{\mathrm{d}\varepsilon_q^p} = D = d_0\left(\exp(m\psi) - \frac{\eta}{M}\right) \tag{A4}$$

The parameter d_0 is determined based on the $d\varepsilon_v$-$d\varepsilon_q$ curve.

(4) Hardening parameters

The parameter n is determined by Equation (14) at a peak stress state, at which K_p=0:

$$n = \frac{1}{\psi^b} ln \frac{M}{M^b} \tag{A5}$$

where ψ^b and M^b are the values of ψ and η at the peak stress state.

Combining Equations (10) (13) and (14) for conventional drained tests (*dp'*=*dq*/3) yields:

$$\frac{\mathrm{d}q}{\mathrm{d}\varepsilon_q} \approx \frac{\mathrm{d}q}{\mathrm{d}\varepsilon_q^p} = \frac{K_p}{1 - {}^{\eta}/_{3}} = h \left\{ \frac{G_0 (2.97 - e)^2 \sqrt{p' p_a} \left(\frac{M}{\eta} - \exp(n\psi) \right)}{(1 + e)(1 - {}^{\eta}/_{3})} \right\} \tag{A6}$$

As all the model parameters in the brackets are known, h is determined based on $\mathrm{d}q - \mathrm{d}\varepsilon_q$ curves along drained triaxial loading paths. Then parameters h_1 and h_2 can be obtained by equation $h = h_1 - h_2 e_0$.